# Inductive Coupling of Power Converter's – EMC

**Irena Kováčová, Dobroslav Kováč**

Faculty of Electrical Engineering and Informatics, Technical University of Košice, Letná 9, 042 00 Košice, Slovak Republik
irena.kovacova@tuke.sk, dobroslav.kovac@tuke.sk

*Abstract: The paper presents a computer analysis of inductive coupling of the electromagnetic compatibility (EMC) problem. Its focus is on power electronics and electrical drives and tests performed by a numerical computer simulation that can disclose suite surprising findings about EMC.*

*Keywords: converters, inductance, electromagnetic compatibility, power electronics*

## 1 Introduction

Importance of electromagnetic compatibility (EMC) of all electrical products has been rapidly growing during the last decade. The environment is increasingly polluted by electromagnetic energy. The interference impact on the surroundings is being doubled every three years and covers a large frequency range.

Equipment disturbances and errors have become more serious as a consequence of the growth of the electronic circuit complexity. According to new technical legislation and also economic consequences, the EMC concept of all products must be strictly observed [1], [2]. It must start with the specification of the equipment performance and end with the equipment installation procedures.

## 2 EMC and Environmental Waste

We all know the environmental pollution problems caused by solid, liquid and gaseous wastes. We are aware of most of these pollutants through our senses.

Due to the increasing life standard, contamination of our environment by the electromagnetic energy is constantly increasing too. Since human beings have no organs for perception of such contamination, they cannot perceive it. The great producers of such waste are electronic systems developed by man and meant to be

effective within these electromagnetic surroundings producing, of course, electromagnetic waste in turn [3].

On one side, interferences are deliberately or involuntarily produced. The place of their origin is called interference source. On the other side, devices may be hindered in their function by such interferences. Those objects are called interference objects.

The possible interfaces between sources and objects are shown in Fig. 1. There are four basic types of coupling that can realize these interfaces.

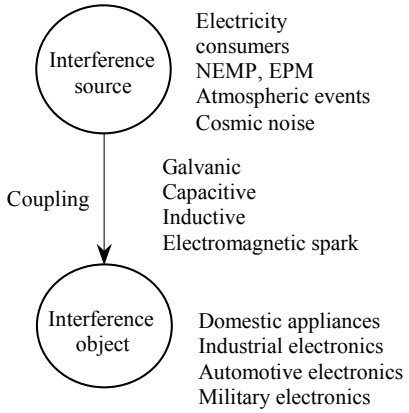


Figure 1
Interference diagram

# 3 EMC – The Interference Mechanism

The interference mechanism can be described in a simplified form as follows. The interference source can be for instance a power semiconductor converter or motor. Interference is produced in the interference source getting into electronics in undesirable ways and is due to various effects distorting signals [4], [5]. Transmission can be direct, for example by galvanic coupling between interference source and interference sink. Interference can be spread through air or via ducts, or coupled inductively or capacitively into signal lines.

Development of power semiconductor elements has caused vehement evolution of the power electronics branch in the last ten years. To investigate the converter functionality, it was necessary first to theoretically analyze and then practically verify its assumed activity. Now, we can eliminate the laborious theoretical analysis by a numerical computer simulation, which can disclose quite surprising findings about EMC.

# 4 Inductive Coupling

Inductive coupling is typical for two and more galvanically separated electric loops at the moment when the smaller one is driven by a time variable- current creating the corresponding, time-variable magnetic field [6], [7]. In such case their mutual intercircuit effect is expressed as a function of the slope of the current increase or decrease, circuit environmental magnetic property as well as circuit geometric dimensions.

To predict the intercircuit inductive coupling, our focus will be on two electric loops $l_1$ and $l_2$ with currents $i_1$ and $i_2$. We will try to determine the effect of loop $l_1$ on loop $l_2$, Fig. 2.

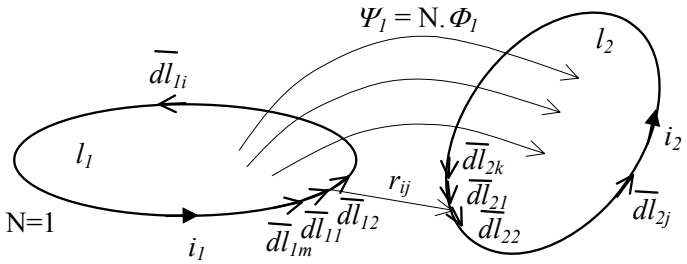


Figure 2
Investigated loops

According to the Maxwell's equation for a quasi-stationary magnetic field:

$$rot\ \overline{E} = -\frac{\partial \overline{B}}{\partial t} \tag{1}$$

and following its integral form: $\int_S rot\ \overline{E}\ d\overline{S} = -\int_S \frac{\partial \overline{B}}{\partial t}\ d\overline{S} = -\frac{\partial}{\partial t}\int_S \overline{B}\ d\overline{S}$ (2)

and after applying the Stoke's theorem, we obtain the equation for the induced voltage:

$$u_{i2} = -\mathrm{N}\frac{\partial \phi_1}{\partial t} = -\frac{\partial \psi_1}{\partial t} = -M\frac{\partial i_1}{\partial t} \tag{3}$$

where $M$ is the coefficient of the mutual inductance. For the magnetic flux $\Psi_1$ definition the equation.

$$\phi_1 = \oint_{l_2} \overline{A}_2\ d\overline{l}_2 \tag{4}$$

Is valid where $\overline{A}_2$ is the vector of the magnetic field potential created by the current $i_1$. We can calculate the value of this vector by the following equation.

$$\overline{A}_2 = \frac{\mu\, i_1}{4\pi} \oint_{l_1} \frac{d\bar{l}_1}{r_{12}} \tag{5}$$

After substituting the last equation with the equation valid for the magnetic flux $\phi_1$, the next relation is obtained:

$$\phi_1 = \oint_{l_2} \left[ \frac{\mu\, i_1}{4\pi} \oint_{l_1} \frac{d\bar{l}_1}{r_{12}} \right] d\bar{l}_2 = \frac{\mu\, i_1}{4\pi} \oint_{l_1} \oint_{l_2} \frac{d\bar{l}_1\, d\bar{l}_2}{r_{12}} \tag{6}$$

and then, $$u_{i2} = -\frac{\partial\left( \frac{\mu\, i_1}{4\pi} \oint_{l_1} \oint_{l_2} \frac{d\bar{l}_1\, d\bar{l}_2}{r_{12}} \right)}{\partial t} = -\frac{\left( \frac{\mu}{4\pi} \oint_{l_1} \oint_{l_2} \frac{d\bar{l}_1\, d\bar{l}_2}{r_{12}} \right) \partial i_1}{\partial t} = -M \frac{\partial i_1}{\partial t}. \tag{7}$$

For the practical use, it is more advantageous to express the induced voltage in the form of a differential [8], [9].

$$u_i = -\frac{di}{dt} \sum_{i=1}^{m} \sum_{j=1}^{k} \frac{\mu}{4\pi} \frac{dl_{1i}.dl_{2j}.\cos\gamma_{dlij}}{r_{ij}} \tag{8}$$

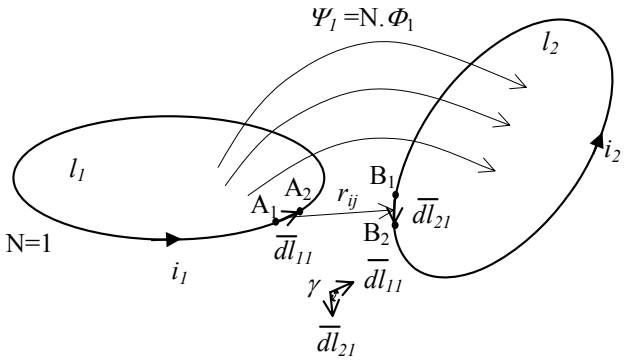


Figure 3
Geometric dimensions of the investigated loops

If we know the geometrical dimensions of the investigated loops Fig. 3 and want to determine their mutual inductive coupling then we can use the next relation (9), (10), (11) for the induced voltage. It is based on the 3D Cartesian coordinate system.

$$u_i = -\frac{di}{dt} \sum_{i=1}^{m} \sum_{j=1}^{k} \frac{\mu}{4\pi} \frac{D+F+G}{\sqrt{O^2+P^2+S^2}} \tag{9}$$

where, $D = (\mathrm{A}_{x2i} - \mathrm{A}_{x1i}).(\mathrm{B}_{x2j} - \mathrm{B}_{x1j})$, (10)

$F = (\mathrm{A}_{y2i} - \mathrm{A}_{y1i}).(\mathrm{B}_{y2j} - \mathrm{B}_{y1j})$, $G = (\mathrm{A}_{z2i} - \mathrm{A}_{z1i}).(\mathrm{B}_{z2j} - \mathrm{B}_{z1j})$,

$$O = \left(\mathrm{B}_{x1j} + \frac{\left|\mathrm{B}_{x2j} - \mathrm{B}_{x1j}\right|}{2}\right) - \left(\mathrm{A}_{x1i} + \frac{\left|\mathrm{A}_{x2i} - \mathrm{A}_{x1i}\right|}{2}\right), \tag{11}$$

$$P = \left(\mathrm{B}_{y1j} + \frac{\left|\mathrm{B}_{y2j} - \mathrm{B}_{y1j}\right|}{2}\right) - \left(\mathrm{A}_{y1i} + \frac{\left|\mathrm{A}_{y2i} - \mathrm{A}_{y1i}\right|}{2}\right), \quad S = \left(\mathrm{B}_{z1j} + \frac{\left|\mathrm{B}_{z2j} - \mathrm{B}_{z1j}\right|}{2}\right) - \left(\mathrm{A}_{z1i} + \frac{\left|\mathrm{A}_{z2i} - \mathrm{A}_{z1i}\right|}{2}\right)$$

For a global solution of the inductive coupling part of the EMC problem inside the overall electric power system [10], [11], it is necessary to analyze the circuit globally paying due regard to the mutual intercircuit inductance coupling. The result is the following integral-differential system of equations.

$$u_{cc1} = R_{c1}.i_1 + L_{c1}.\frac{di_1}{dt} + \frac{1}{C_{c1}}\int i_1.dt + \sum_{\substack{j=1 \\ j\neq 1}}^{k} u_{ij} \tag{12}$$

$$\vdots$$

$$u_{cck} = R_{ck}.i_k + L_{ck}.\frac{di_k}{dt} + \frac{1}{C_{ck}}\int i_k.dt + \sum_{\substack{j=1 \\ j\neq k}}^{k} u_{ij} \tag{13}$$

For this purpose it is very suitable to explore the existing simulation programs such as for instance the PSPICE program utilized worldwide [12], [13], [14].

In the next part, we will try to determine the effect of the one-quadrant impulse converter on the sensing circuit as it shown in Fig. 4. The circuit dimensions are $a = 0.2$ m, $b = 0.3$ m, $c = 0.1$ m, $d = 0.05$ m, $e = 0.005$ m. The radius of the copper wires is $R = 0.0006$ m and the relative permitivity of the circuit environment is $\mu_r = 0.991$.

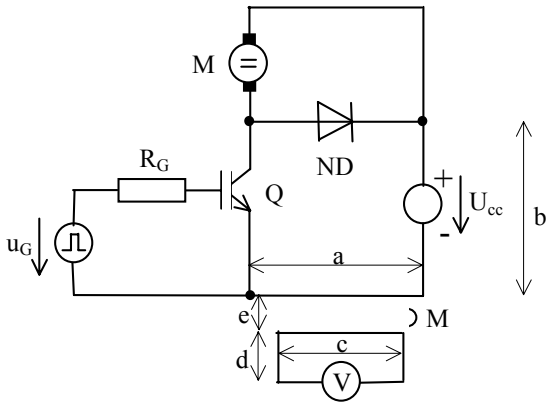


Figure 4
Investigated circuit

The inductance of the first loop is given as (14) and of the second as (15).

$$L_1 = L_{e1} + L_{i1} = \frac{\mu_0 b}{\pi}\ln\frac{a-R}{R} + \frac{\mu_0 a}{\pi}\ln\frac{b-R}{R} + \frac{\mu.2.(a+b)}{8\pi} = 1.294\,\mu H \tag{14}$$

$$L_2 = L_{e2} + L_{i2} = \frac{\mu_0 c}{\pi}\ln\frac{d-R}{R} + \frac{\mu_0 d}{\pi}\ln\frac{c-R}{R} + \frac{\mu.2.(c+d)}{8\pi} = 0.294\mu H \tag{15}$$

The mutual inductance $M$ calculated from the above mentioned equation is $M = 477.4$ nH. The magnetic coupling coefficient $k$ is given as:

$$k = \frac{M}{\sqrt{L_1 + L_2}} = 0.774\,. \tag{16}$$

Now we can use the PSPICE simulation program for solving the inductive coupling problem between the two circuits [15], [16]. Parameters of the circuit simulation are $R_Z = 11.66\ \Omega$, $L_Z = 400\ \mu$H, $R = 10\ \Omega$, $R_G = 100\ \Omega$ and $U_{CC} = 70$V. The schematic connection is shown in Fig. 5. The IGBT transistor Q was switched on at the frequency 10 kHz and the switch on/off ratio was 0.5.

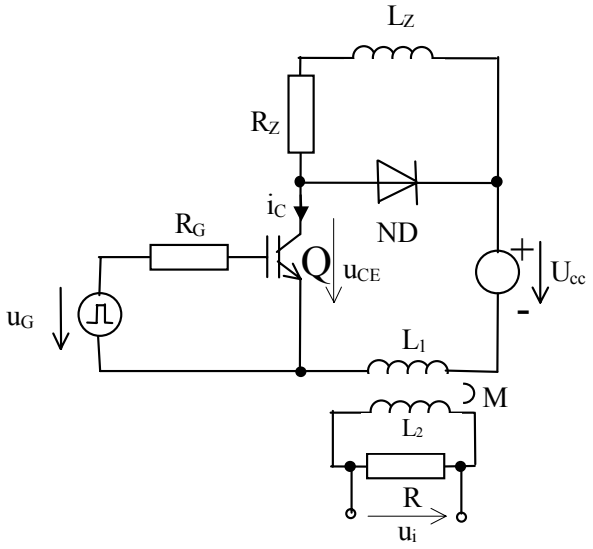


Figure 5
Simulation circuit

Simulation results are shown in Fig. 6. Results obtained by measurements are shown in Figs. 7 and 8 and switching details in Figs. 9 and 10, where damping transient resonant state created by parasitic transistor capacitances, parasitic conductor inductance and transistor internal resistance causes undulation of the waves of current $i_C$ and voltage $u_{CE}$.

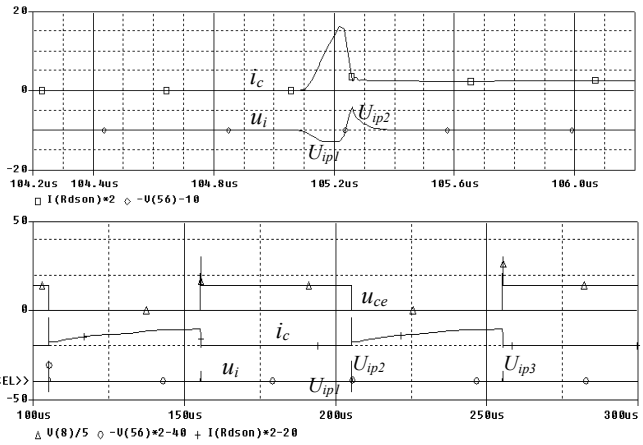


Figure 6
Simulation results

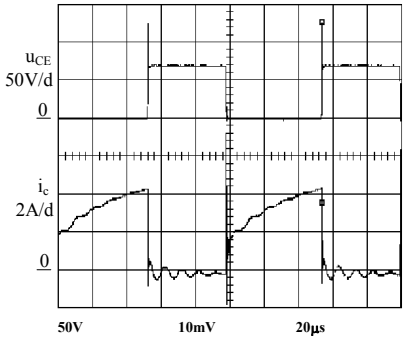


Figure 7
Measured voltage $u_{CE}$ and current $i_C$

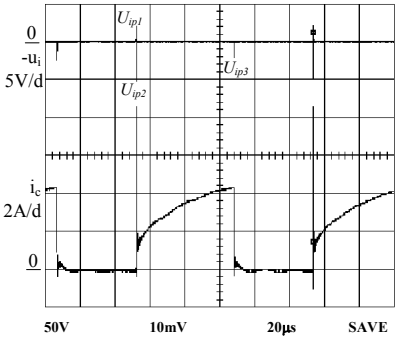


Figure 8
Measured voltage $-u_i$ and current $i_C$

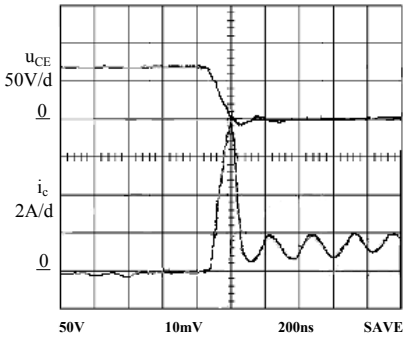


Figure 9
Switching on voltage $u_{CE}$ and current $i_C$

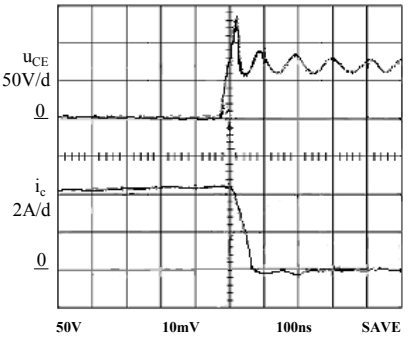


Figure 10
Switching off voltage $u_{CE}$ and current $i_C$

A comparison of the simulated and measured results shows that peaks of transistor current *ic* have the same values, that is 8.4 A, in both cases. The same values, that is 4.4 A, have both the simulated and measured transistor current at the moment when transistor is switched off. There is a small difference only between the simulated and measured curves of the transistor voltage $u_{CE}$. The overvoltage generated at the transistor switching off reaches the value of 150 V for the simulated result. However, the corresponding overvoltage has only the value of 130 V for the measured result. Peaks of the simulated and measured induced voltages have the same values of $U_{i1}$ = -2.2V, $U_{i2}$ = 5.02V, $U_{i1}$ = 2.1V. This means that such method is acceptable for inductive coupling investigation of the EMC problem.

To improve the obtained results, the numerical solution of the magnetic field by finite element method program was also used [17]. The result of such analysis is shown in Fig. 11.

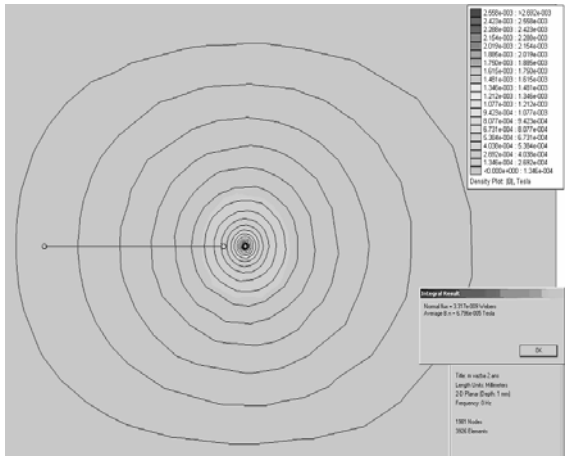

Figure 11
The finite element simulation method of the magnetic field

From the "integral result" data window it is seen, that the value of the magnetic flux inside the sensing circuit is $3.317 \times 10^{-9}$ Wb. Based on the basic program property allowing semi-real 3D space simulation with the third dimension equal only to the basic unit of the depth (1 mm), we multiplied the obtained value of the magnetic flux by the value of the sensing circuit depth c = 100 mm. The total magnetic flux was then $331.7 \times 10^{-9}$ Wb. This flux was excited by the peak circuit current 8.4 A, the rising time of which was 140 ns. On the basis of the above equations, the first peak of the induced voltage can be calculated as:

$$U_{ip1} = \frac{\Delta \Phi_1}{\Delta t_1} = \frac{0 - 331.7 \times 10^{-9}}{140 \times 10^{-9}} = \frac{-331.7 \times 10^{-9}}{140 \times 10^{-9}} = -2.369 \text{ V} . \qquad (17)$$

Similarly, it is possible to calculate the rest of the peaks of the induced voltage $u_i$:

$$U_{ip2} = \frac{\Delta\Phi_2}{\Delta t_2} = \frac{331.7 \text{ x } 10^{-9} - 55.3 \text{ x } 10^{-9}}{55 \text{ x } 10^{-9}} = \frac{276.4 \text{ x } 10^{-9}}{55 \text{ x } 10^{-9}} = 5.025 \text{ V} \tag{18}$$

$$U_{ip3} = \frac{\Delta\Phi_3}{\Delta t_3} = \frac{173 .7 \text{ x } 10^{-9} - 0}{80 \text{ x } 10^{-9}} = \frac{173 .7 \text{ x } 10^{-9}}{80 \text{ x } 10^{-9}} = 2.171 \text{ V} . \tag{19}$$

The results obtained by the finite element numerical simulation method are again confirming the correctness of the above mentioned methods.

# 5 Electric Motor Interference Simulation

The following interference simulation investigation was done by electric motor, which also can be representing the interference source. The transmission of interference can be direct via galvanic coupling or can be propagated through the air or via ducts with electromagnetic field.

Electric motors can be divided by course of rotor design and course of magnetic flux in regard to motor axle into two series:

1 Standard motors with radial magnetic flux.

2 Disc motors with axial magnetic flux.

For the drives, which needs to have a great dynamics, is possible to choice the motor from the group of disc motors. As consequence of the fact that magnetic flux in disc motor have axial direction, the stray flux to the surroundings of such motors is generally greater than stray flux of classic motor with cylindrical rotor. In due to requirement of extension of motor torque these motors have generally double-sided stator (on both of them side discoid curl). The air gap is also divided on two sections, the dimensions of which have important influence on the total stray flux in the area of air gap.

By improving of all electromagnetic construction motor parameters we will obtain the motor with the higher power. But such motor will be also representing the source with higher interference. Because these motors are used as a part of the more complicated equipments with serious electronic control, so their backward influence on control unit must be as smallest as possible and such a way it will be possible to avoid of EMC equipment troubles. Study of EMC of such electrical drives has more and more bigger importance for praxis.

EMC investigation is possible to do either by measures of real motor parameters or easier and more economically by computer simulation [18], [19]. The task is then to create real computer simulation model of interference source [20], [21]. In

our case such source will represent the disc motor. Simplified electromagnetic, two dimensional model of such disc motor was developed. Magnetic field investigation was done by student version of Qfield program. The simplified simulation model of disc motor with enquired magnetic field is shown on Fig. 12.

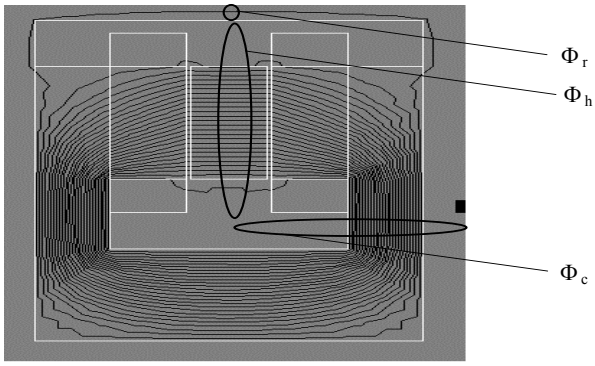


Figure 12
Magnetic field calculation

The EMC quality of designed disc motor we can state on the basis of difference of two magnetic fluxes. First magnetic flux $\Phi_c$ is representing total magnetic flux produced by motor. Its value is depending on the motor power. The second (main) magnetic flux $\Phi_h$ represents the part of the total magnetic flux, which is closed only through magnetic circuit of disc motor. By the difference of the total and main magnetic fluxes we can obtain stray magnetic flux $\Phi_r$, which is closed outside of the motor in surrounding space. This magnetic flux represents the real source of interference.

The motor frame material and its dimensions have important influence on motor stray field. According this fact the simulation analysis was done for stating of magnetic flux dependencies on motor frame materials and its dimensions. Results are presented in Tables 1 and 2. Table 2 presents results for aluminum frame.

Table 1
Magnetic fluxes inside motor frame materials

| Motor frame size (L) is 3.8 mm | | | |
|---|---|---|---|
| Material | $\Phi_c$ [Wb] | $\Phi_h$ [Wb] | $\Phi_r$ [%] |
| Al | 0.026627 | 0.025885 | 2.87 |
| Steel1511 | 0.03283 | 0.025088 | 30.86 |
| Steel1211 | 0.033323 | 0.025081 | 32.86 |
| Steel St3 | 0.03381 | 0.025082 | 34.78 |

Table 2
Magnetic fluxes for different material thicknesses

| L [mm] | $\Phi_c$ [Wb] | $\Phi_h$ [Wb] | $\Phi_r$ [%] |
|---|---|---|---|
| 3.8 | 0.026627 | 0.025885 | 2.87 |
| 1.6 | 0.026156 | 0.025099 | 4.21 |

In following we will suppose only change of the current density ($J$) in motor excitation coil. Results of magnetic field analyses under such conditions are presented in Table 3.

Table 3
Magnetic fluxes for different current densities

| J[A.m$^{-2}$.10$^6$] | $\Phi_c$ [Wb] | $\Phi_h$ [Wb] | $\Phi_r$ [%] |
|---|---|---|---|
| 2.67 | 0.014945 | 0.014342 | 4.20 |
| 4.67 | 0.026156 | 0.025099 | 4.21 |
| 6.00 | 0.033626 | 0.03226 | 4.23 |

## Conclusions

Although the investigated example seems to be not very realistic so we must take into consideration also the following four conclusions. The first one is that the presented example is very simple for demonstration of EMC consequences. The second one is that the real dimensions of the converter circuits are obviously in millimeters and so the circuit area is smaller in comparison with demonstration example, but we should take into consideration also the opposite influence resulting from the shorter switching times. Such a way the realistic final result could be that the induced voltages will reach values of few tenths of millivolts in real equipments. The third conclusion is that induced voltage in real equipment is created as sum of more circuit interactions and so it can reach also range of the volts. The fourth one is that also low-level induced voltage can have the important impact on properly work of some circuits (for example microprocessors, etc.). However the main contribution of performed analyses consist in derivation of equations by which any inductive coupling EMC problem is possible simply analyse by computer numerical method.

## Acknowledgement

The paper has been prepared by the support of Slovak grant projects VEGA No. 1/4174/07, 1/0660/08, KEGA 3/5227/07, 3/6388/08, 3/6386/08.

## References

[1] I. Kováčová, D. Kováč, J. Kaňuch: EMC from the Look of Theory and Application. *BEN - technical literature Publisher*, Prague, 2006

[2] D. J. Carpenter: EMC Emissions Certification for Large Systems - A Risk Management Approach. *BT Technology Journal*, Vol. 21, No. 2, pp. 67-76, 2003

[3] I. Tomčíková, J. Molnár, T. Vince*:* Interaction of Magnetic Field and Tenseness for Elastomagnetic Sensor of Pressure Force. *Elektrorevue*. No. 34, 2008, pp. 1-11

[4] L. Madarász: Intelligent Technologies and their Applications in the Large-Scale Systems. *University Press Elfa*, ISBN 80-89066-75-5, 346, pp., Košice, 2004

[5] I. Tomčíková: Magnetic Field Solving of Elastomagnetic Sensor of Pressure Force. Electroscope. No. 4, 2008

[6] I. Kováčová, D. Kováč, J. Kaňuch: EMC of Power Electrotechnical Systems. *Equilibria Publisher*, Košice, 2005

[7] I. Kováčová, D. Kováč: Electromagnetic Coupling - EMC of Electrical Systems (Part I). *International Review of Electrical Engineering*, Vol. 1, No. 2, pp. 234-240, 2006

[8] M. Orendáč, I. Tomčíková: Basics of Electrical Engineering. Lectures and exercises. *Elfa Publisher*, Košice, 2005

[9] I. Kováčová, D. Kováč: Electric Power Systems – EMC. *Advances in Electrical and Electronic Engineering*, Vol. 5, No. 3, pp. 392-395, 2006

[10] I. Kováčová, D. Kováč: Power transistors MOSFET and IGBT. *Elfa Publisher*, Košice, 1996

[11] I. Kováčová, D. Kováč: EMC Compatibility of Power Semiconductor Converters and Inverters. *Acta Electrotechnica et Informatica*, Vol. 3, No. 2, pp. 12-14, 2003

[12] J. K. Tar, I. J. Rudas, L. Madarász, J. F. Bitó: Simultaneous Optimalization of the External Loop Parameters in an Adaptive Control Based on the Co-operation of Uniform Procedures. *Journal of Advanced Computational Intelligence,* No. 4, pp. 279-285, 2000

[13] P. Špánik, B. Dobrucký, M. Frívaldský, P. Drgoňa: Experimental Analysis of Commutation Process of Power Transistor Structures. *Acta Technica CSAV*, Vol. 52, No. 4, pp. 399-413, 2007

[14] H. Göksu, D. C. Wunsh: Neural Networks Applied to Electromagnetic Compatibility Simulations. *Lecture Notes in Computer Science*, Vol. 2714, pp. 1057-1063, 2003

[15] D. Mayer, B. Ulrych, M. Škopek: Electromagnetic Field Analysis by Modern Software Products. *Journal of Eletrical Engineering*, Vol. 7, No. 1, 2001

[16] J. C. Fodor: Contrapozitive Symmetry of Fuzzy Implications. *Fuzzy Sets and Systems 69*, pp. 141-148, 1995

[17] I. Kováčová, J. Kaňuch, D. Kováč: DC Permanent Magnet Disc Motor Design with Improved EMC. *Acta Technica CSAV*, Vol. 50, No. 3, pp. 291-306, 2005

[18] J. K. Tar, I. J. Rudas, J. F. Bitó, J. A. T. Machado: Centralized and Decentralized Applications of a Novel Adaptive Control. *In Proceeding of IEEE 9th International Conference on Intelligent Engineering Systems (INES 2005)*, Cruising on Mediterranean Sea, pp. 87-92, Sept. 16-19, 2005

[19] T. Vince, J. Molnár, I. Tomčíková: *Remote DC Motor Speed Regulation via Internet*. 10th Int. PhD Workshop OWD 2008, Warszawa, pp. 293-296, 2008

[20] V. Olej, P. Hajek: Hierarchical Structure of Fuzzy Inference Systems Design for Municipal Creditworthiness Modelling, *WSEAS Transactions on Systems and Control, Issue 2, Vol. 2*, February 2007, ISSN 1991-8763, pp. 162-169

[21] R. Andoga, L. Madarász, L. Főző: Situational Modeling and Control of a Small Turbojet Engine MPM 20. *IEEE 4th International Conference on Computational Cybernetics (ICCC 2006)* August 20-22, 2006, Tallin, Estonia, pp. 81-85, ISBN 1-4244-0071-6